CHEMISTRY OF MATERIALS

Article

pubs.acs.org/cm

Improving the Performance of High Capacity Li-Ion Anode Materials by Lithium Titanate Surface Coating

Ge Ji, Yue Ma, Bo Ding, and Jim Yang Lee*

Department of Chemical and Biomolecular Engineering, National University of Singapore, 10 Kent Ridge Crescent, Singapore 119260

Supporting Information

ABSTRACT: Current methods for improving the electrochemical performance of lithium-ion battery electrode materials mostly depend on materials design and synthesis. We propose that the unique electrochemical properties of spinel lithium titanate ($Li_4Ti_5O_{12}$, LTO) make it suitable as a protective coating to improve the performance of high capacity anode materials. In this study, tin oxide was coated with LTO to reduce the initial irreversible capacity loss because of solid electrolyte interface (SEI) formation and to improve the reversibility (capacity and rate performance) of tin oxide for Li^+ storage. The LTO coating was applied to porous hollow tin oxide particles by a two-step process. Experimental measurements showed that the LTO coating shielded most of the direct contact between tin oxide and the electrolyte and hence the ICL due to SEI formation was reduced to mostly that of LTO, which is much lower than tin oxide. In addition the coated tin oxide also showed notable improvements in material cyclability and rate performance.

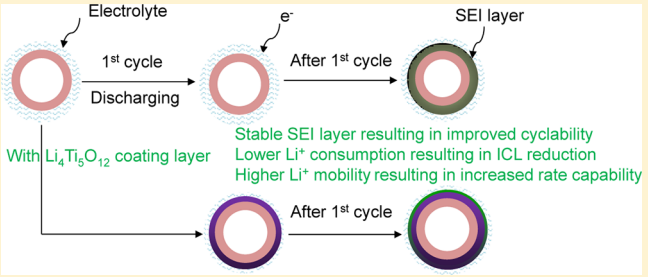

KEYWORDS: *core−shell, lithium titanate, Li ion batteries, tin oxide*

1. INTRODUCTION

The current interest in electric vehicles and energy storage for grid-scale applications has driven up the demand for high energy density lithium-ion batteries (LiONs). Materials innovations are still the most promising approach to deliver the necessary technology breakthrough. Lithium-alloying elements such as tin and silicon can easily increase the Li^+ storage capacity of the anode by a factor of two to ten over the current carbon-based anodes. However, the development of these high-capacity anode materials has been met with two significant challenges: high initial capacity loss (ICL) and poor capacity retention in prolonged cycling.[1−4] ICL is caused by irreversible secondary reactions such as the formation of a solid electrolyte interface (SEI).[5] Poor capacity retention is generally attributed to the large volume excursion in lithium insertion and extraction reactions, which predisposes the anode to cracking and loss of electrical connectivity.[6] The solution to these two problems is continually being improved through materials design and preparation.[7−17] For example, nanostructuring has been used to reduce the Li^+ diffusion length and to increase the tolerance to strains caused by the Li^+ insertion/extraction reactions.[2,18−20] Compositing the active material with a softer matrix capable of stress absorption is another approach.[7−9,21−25] For the latter carbon has been the most commonly used compositing medium. Because of the generally low graphitization degree of carbon in the composite, the ICL of the composite is often rather large.[4,26−28] Other composites such like SnO_2/TiO_2,[29] Si/SnO_2[30] have also been investigated as anode materials for the LiONs.

SnO_2 has a high Li^+ storage capacity (781 mAh/g according to the following reactions: $SnO_2 + 4Li^+ + 4e^- \rightarrow Sn + 2Li_2O$, $Sn + xLi^+ + xe^- \rightarrow Li_xSn$ $(0 \le x \le 4.4)$) and is relatively easy to synthesize by environmentally friendly methods from low cost resources.[31] Hence it has been extensively studied as an anode material for LiONs. Spinel lithium titanate ($Li_4Ti_5O_{12}$, LTO) was also identified as an alternative anode material. It has very good reversibility (it incurs zero strain in Li insertion and extraction reactions) and excellent rate performance, and no SEI formation in the 1.0−2.0 V voltage window.[32] SEI, however, does form at potentials below 1.0 V.[33,34] Cycling LTO between 0.0−2.0 V was found to cause a first cycle ICL of about 70 mAh/g but capacity in this lower potential region was stable from the second cycle onward.[34] $SnO_2/Li_4Ti_5O_{12}$[35] and $Sn/Li_4Ti_5O_{12}$[36,37] composites have been explored as anode materials before but the composites in these early studies were random mixtures and as a result the electrochemical performance was not satisfactory. The specific capacity was generally rather low (the highest charge capacity in the first cycle was 321 mAh/g). We hypothesize that LTO could be used more effectively as a protective coating on high capacity anode materials to reduce the ICL and to concurrently improve the electrochemical performance of the latter. LTO has several advantages as a protective coating. First, compared with high quality carbon coatings which can only be prepared at high

Received: March 25, 2012
Revised: August 3, 2012
Published: August 7, 2012

temperature or pressure in an inert atmosphere, a LTO coating can be prepared in air at lower temperatures;[32] Second, LTO with its high Li^+ mobility[38] may also facilitate the transport of Li^+ to the active material, and hence improving the rate capability of the active material.

The viability of using LTO to decrease the ICL and to improve other aspects of tin oxide particles in LiON applications is investigated in this study. SnO_2 is very amenable to the LTO modification. Specifically, tin oxide particles with a hollow core and a porous shell aggregated from primary tin oxide nanoparticles (NPs) were used as the active Li^+ storage compound. The hollow interior and the porosity in the shell provided the space for volume excursion in Li−Sn reactions during discharging and charging. The LTO coating shielded most of the direct contact between tin oxide and the electrolyte and as such the ICL due to SEI formation was reduced to that of LTO. The SEI formed was also more stable than that on a native Sn-based anode resulting in some cyclability improvement. Furthermore, there was also an increase in the rate performance. Figure 1 is a simplified illustration of the advantages of LTO surface coating.

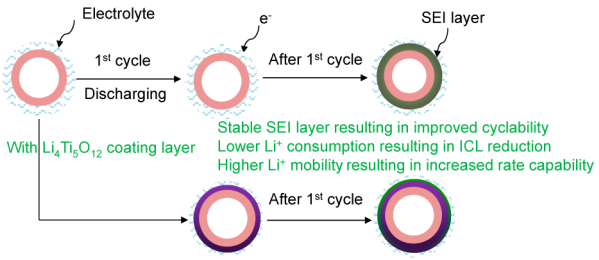

Figure 1. Schematic illustration showing hollow tin oxide particles with and without the LTO coating. For the uncoated hollow tin oxide particles, an unstable SEI layer is formed in the 1st cycle resulting in a large irreversible consumption of Li^+ ions. With the LTO coating, a more stable SEI layer is formed in the 1st cycle; reducing the irreversible consumption of Li^+ ions and also improving material cyclability. The high Li^+ mobility in LTO could also facilitate Li^+ transport to the core to increase rate performance.

2. EXPERIMENTAL SECTION

2.1. Preparation of Hollow $SnO_2/Li_4Ti_5O_{12}$ Core−Shell Composite Particles. Hollow tin oxide NPs were prepared by the Lou method[3] with some modifications. Specifically calculated amounts of urea and potassium stannate trihydrate ($K_2SnO_3{\cdot}3H_2O$) were dissolved in 35 mL of an ethanol/water mixture (40% ethanol by volume) to final concentrations of 0.1 M and 16 mM respectively. After the mixture was stirred for 5 min and aged for 40 min, a white translucent solution was formed. The solution was transferred to a 50 mL Teflon lined stainless steel reactor and hydrothermally treated at 150 °C for 24 h. A white precipitate was formed which could be recovered by centrifugation followed by washing with ethanol and deionized water, and drying in vacuum at 50 °C for 12 h.

The hollow tin oxide NPs formed by the above procedures were deposited with titantia by two methods. In the first method, 1 g titanium isopropoxide (TTIP) was dissolved in 30 mL of ethanol and stirred for 2 min. Hollow tin oxide (0.5 g) was added to the TTIP solution and ultrasonicated for 15 min. After it was stirred for 0.5 h, the mixture was placed on an orbital shaker and incubated for 12 h. The mixture was then centrifuged to remove the excess titania sol. The solid-phase separated as such was condensed with ethanol/water (1:1) under magnetic stirring for 2 h at room temperature. The final sediment was collected by centrifugation and washed with deionized water and ethanol. It was then vacuum-dried at 50 °C for 12 h.

The second coating method was based on the procedure of Tang.[39] In this case, 0.2 g hollow tin oxide was ultrasonically dispersed in 40 mL of a ethanol/acetonitrile mixture (3:1 v/v). 0.3 mL ammonia solution (32%) was then added under vigorous stirring at room temperature. Finally, 0.5 − 0.8 mL of titanium tetrabutoxide (TBOT) in 10 mL ethanol/acetonitrile (3:1 v/v) was slowly introduced to the above suspension with stirring. After stirring for 2 h, the solid product was recovered by centrifugation followed by washing with deionized water twice. It was then dried in a vacuum oven at 50 °C for 12 h.

The titania coating was then converted to a lithium titanate shell by the following procedure: 6 mmol LiOH was dissolved in 30 mL deionized water with stirring. The titania-coated hollow tin oxide NPs were ultrasonically dispersed in the LiOH aqueous solution. The mixture was transferred to a 50 mL Teflon-lined reactor and sealed. The reactor was heated to 180 °C and kept at this temperature for 20 h to form a lithium titanate coating on the hollow tin oxide particles. The solid phase was recovered by centrifugation followed by washing with ethanol and deionized water; and vacuum drying at 50 °C for 12 h. The final product was obtained after calcination at 800 °C for 2 h.

2.2. Characterization. The intermediate and final products prepared above were characterized by field-emission scanning electron microscopy (FESEM) and scanning transmission electron microscopy (STEM) on a JEOL JSM-6700F operating at 5 and 25 kV, respectively. High-resolution TEM (HRTEM) and EDX were performed on a Philips FEG-CM300 operating at 200 kV. Powder X-ray diffraction (XRD) was recorded on a Shimadu XRD-6000 using Cu Kα radiation. Cyclic voltammetry was performed on an AutoLab Electrochemical System in the 0−3 V window at 0.2 mV/s.

2.3. Electrochemical Measurements. The candidate anode material was mixed with 10 wt % polyvinylidene fluoride (PVDF) binder and 10 wt % Super P (Timcal) in *N*-methylpyrrolidone (NMP) into a homogeneous slurry. The slurry was applied to a copper disk current collector and dried in vacuum at 120 °C overnight. Li test cells were assembled in an argon-filled glovebox using a lithium metal foil (Li metal is reactive to H_2O and air and must be handled with care) doubled as the counter and reference electrodes; and 1 M $LiPF_6$/ EC + DEC (1:1 w/w) as the electrolyte. The cells were tested on a Maccor Series 2000 battery tester at ambient conditions at constant discharge and charge current densities in the 5 mV to 2 V voltage window.

3. RESULTS AND DISCUSSION

Hydrothermal processing was selected in this project to construct the designed core−shell structure. Classical epitaxial deposition or solution deposition method was unable to achieve the same in this case. This is because LTO could only be formed under high temperature or high pressure conditions, making it difficult to apply the usual kinetic control strategy for the heterogeneous nucleation of the shell on the core. The LTO coating was prepared by a two-step process: a titania shell was first created by the hydrolysis−condensation of titanium alkoxide in the presence of preformed tin oxide nanoparticles. It was then converted into LTO by reacting with LiOH under hydrothermal conditions.

The major steps in the preparation process and the evolution of the composite are illustrated in Figure 2a. Hollow tin oxide NPs were first prepared by a template-free method[3] which involved the hydrothermal treatment of stannate in an ethanol−water mixture and inside−out Ostwald ripening. Titania was then coated on the exterior of the preformed tin oxide NPs by controlling the hydrolysis rate of titanium isopropoxide (TTIP) or titanium tetrabutoxide (TBOT). A LTO shell was then formed by the reaction between the titania shell and lithium hydroxide in water at 180 °C under hydrothermal conditions for 20 h. In the last process, excess LiOH was used to ensure the complete conversion of titania to LTO. Finally, the SnO_2@$Li_4Ti_5O_{12}$ core−shell composites were

dx.doi.org/10.1021/cm301432w | *Chem. Mater.* 2012, 24, 3329−3334

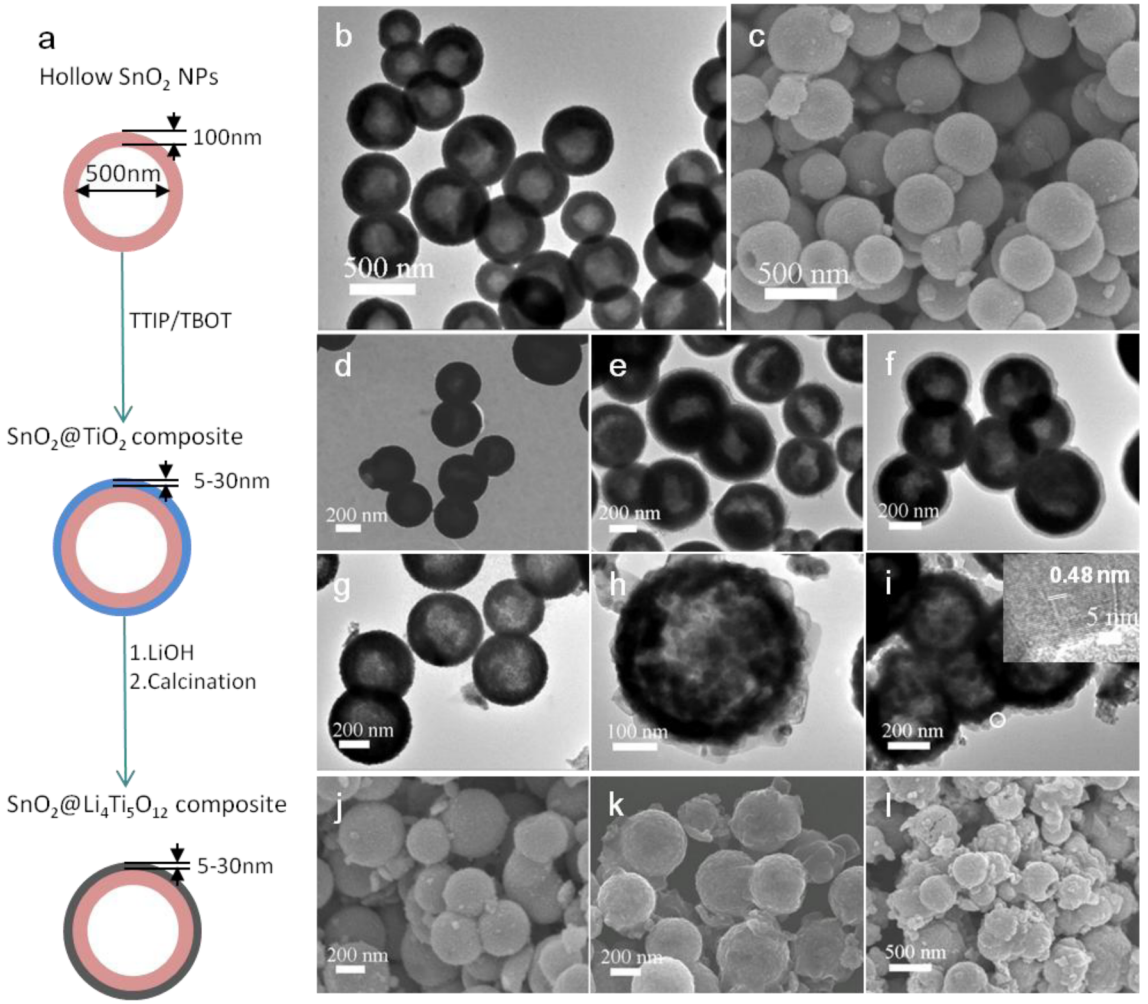

Figure 2. (a) Evolution of the SnO_2@$Li_4Ti_5O_{12}$ core−shell composite, (b-l) morphologies of intermediate and final products. (b, e-i) TEM, (d) STEM, and (c, j-l) SEM micrographs of (b, c) pristine hollow tin oxide nanoparticles, (d) SO/TO-5, (e) SO/TO-15, (f) SO/TO-30, (g, j) SO/LTO-5, (h, k) SO/LTO-15, and (i, l) SO/LTO-30. The inset in panel I shows the circled region at higher magnification.

calcined in air to increase the crystallinity of the final composite product.

Figure 2b and c shows typical TEM (b) and SEM (c) images of the SnO_2 NPs. These spherical hollow NPs were 300−800 nm in size with a shell thickness of 50−150 nm. Upon closer examination the shell was found to be aggregated from small primary NPs about 10 nm in diameter (Figure 2c). For the first coating method, the hollow SnO_2 NPs were aged in a titantia sol for 12 h and then condensed by an ethanol/water mixture (labeled as SO/TO-5). A thin uniform coating could be confirmed by STEM imaging (Figure 2d). The thickness of the coating on the SnO_2 NPs was estimated to be about 5 nm. Because of the low affinity between tin oxide and TTIP, the coating formed by this method was relatively thin. A thicker uniform coating layer could however be formed by the Tang's method.[39] Here stable SnO_2@TiO_2 core−shell particles were prepared by the hydrolysis of TBOT catalyzed by ammonium ions in the mixed solvent (labeled as SO/TO-15 and SO/TO-30). The thickness of the coating could be varied by controlling the amount of TBOT used (0.5 mL for SO/TO-15 and 0.8 mL for SO/TO-30). In the TEM images of SO/TO-15 and SO/TO-30 in Figure 2e, f; a shell thickness of 15 nm for SO/TO-15 and 30 nm for SO/TO-30 could be measured. The titania coating also imparted a smoother texture to the hollow tin oxide particle exterior. This could be explained by the adsorption of NH_4^+ on the surface of the tin oxide particles, enabling a more uniform distribution of the negatively charged titania precursor in the surrounding and consequently a more homogeneous condensation process leading to uniform deposition. The uniform coating was formed under diffusion-controlled kinetics with the mixed solvent controlling the rate of diffusion of the titania precursor.

In the final step of the preparation SO/TO-5, SO/TO-15, and SO/TO-30 were reacted with LiOH and calcined to form SnO_2@$Li_4Ti_5O_{12}$ core−shell composites (labeled as SO/LTO-5, SO/LTO-15 and SO/LTO-30 respectively). The morphology of the thin shelled SO/LTO-5 composite is shown in Figure 2g, j. The LTO coating could not be easily identified because of the thinness of the shell. The LTO coating was more visible in SO/LTO-15 and SO/LTO-30. TEM (Figure 2h, i) estimated thickness of ∼15 nm for SO/LTO-15 and 30 nm for SO/LTO-30. The uniformity of the coating was also confirmed. In the HRTEM mode, lattice fringes could also be detected in the coating on SO/LTO-30. The interplanar spacing of 4.8 Å corresponds well with the $Li_4Ti_5O_{12}$ (111) planes. SEM examination (Figure 2j−l) revealed more particle rupture in SO/LTO-15 and SO/LTO-30 than SO/LTO-5. This was most likely caused by the differential expansion of the core and shell

dx.doi.org/10.1021/cm301432w | *Chem. Mater.* 2012, 24, 3329−3334

components during hydrothermal processing, which was more severe in composites with a thicker shell.

The core−shell structure and the composition of the composite were also confirmed by other methods. The element maps from energy-dispersive X-ray (EDX) spectroscopy were used to ascertain the core−shell structure. Using SO/LTO-30 as a typical example, three SO/LTO-30 particles were used to sample the distributions of tin, oxygen and titanium. Figure 3a shows that the presence of titanium was confined to the shell area. A line scan image further confirmed the concentration of Ti in the shell area outside the hollow SnO_2 core (Supporting Information, Figure S1). The Ti:Sn ratios in SO/LTO-5, SO/LTO-15, and SO/LTO-30 were determined to be 1:33, 1:5.7, and 1:4.2 by EDX, consistent with the increasingly thicker shells. The corresponding weight fractions of LTO in these composites were 1.8%, 9.7%, and 12.7% respectively. X-ray diffraction (XRD) was used to determine the material phases in SO@LTO. All the peaks in the XRD pattern of calcined hollow tin oxide spheres (800 °C for 2 h in air, labeled as SO in Figure 3b, could be indexed to crystalline SnO_2 (cassiterite, JCPDS Card No. 41-1445). The broad fwhm (full width at half-maximum) of the diffraction peaks is indication of the smallness of the constituent primary crystalline SnO_2 NPs. For the $SnO_2@Li_4Ti_5O_{12}$ composite, four additional peaks appeared at 18.5°, 35.6°, 43.4°, and 62.9°, which correspond well with the (111), (311), (400), and (440) diffractions of spinel lithium titanate (JCPDS Card No. 26-1198). The intensity of these LTO peaks increased as the thickness of the coated layer increased.

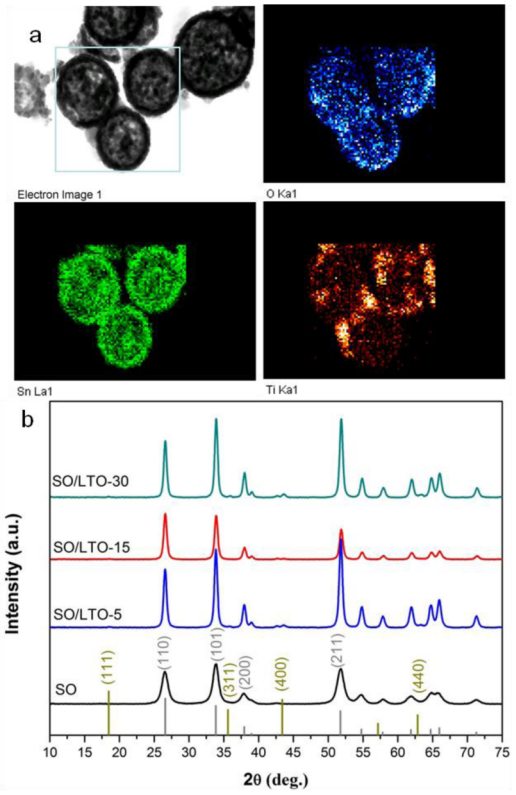

Figure 3. (a) Element mapping of SO/LTO-30 and (b) XRD patterns of SO, SO/LTO-5, SO/LTO-15, and SO/LTO-30. The vertical lines are the standard XRD patterns of cassiterite SnO_2 (JCPDS Card No. 41-1445) (gray line) and spinel lithium titanate (JCPDS Card No. 26-1198) (yellow line).

For the examination of the effects of LTO coating on the electrochemical performance of SnO_2, hollow tin oxide NPs after calcination (800 °C for 2 h in air) and $SnO_2@Li_4Ti_5O_{12}$ composites with different shell thicknesses were used as the anodes in half cell measurements. Testing was carried out under constant current conditions (100 mA/g) in the 5 mV−2 V voltage at room temperature. The first cycle discharge (Li^+ insertion) and charge (Li^+ extraction) capacities and ICL for each of these materials are summarized in Table 1. Figure 4a shows the first cycle discharge/charge curves of pristine hollow tin oxide and SO/LTO-15 (the first cycle discharge/charge curves of other $SnO_2@Li_4Ti_5O_{12}$ composites are similar in features). The first cycle charge and discharge capacities of SO/LTO-15 were 600.0 and 1030.9 mAh/g respectively, while the corresponding values for the uncoated SnO_2 hollow NPs were 614.3 and 1340.0 mAh/g measured at the same current density. The overall ICL therefore decreased from 725.7 to 430.9 mAh/g. The voltage plateau around 1.0−0.8 V for the hollow tin oxide and around 0.9−0.7 V for the $SnO_2@Li_4Ti_5O_{12}$ composite in the discharge curves of Figure 4a could be attributed to the reduction of tin oxide to tin.[1,40] The corresponding ICL as measured from Figure 4a for the hollow tin oxide NPs was 300 mAh/g. Since the $SnO_2@Li_4Ti_5O_{12}$ composite contained both Sn and Ti, the ICL corresponding to the reduction of tin oxide to tin in $SnO_2@Li_4Ti_5O_{12}$ was calculated from the measured values by the equation below.

$$C_{\text{reduction of tin oxide to tin}} = \frac{300\ \frac{\text{mAh}}{\text{g}} \times R \times \frac{150.71\ \text{g}}{\text{mol}}}{R \times \frac{150.71\ \text{g}}{\text{mol}} + \frac{1}{5} \times \frac{459.1\ \text{g}}{\text{mol}}}$$

In the equation, R is the atomic ratio of Sn:Ti in the $SnO_2@Li_4Ti_5O_{12}$ composite, and 150.71 g/mol and 459.1 g/mol are the molecular weights of SnO_2 and $Li_4Ti_5O_{12}$, respectively.

The ICL due to SEI formation could then be calculated as the difference between the measured ICL and the ICL attributable to tin oxide reduction. The calculated values were 425.7 mAh/g for the hollow tin oxide NPs and 159.5 mAh/g

Table 1. Summary of Electrochemical Performance of SO and SO/LTO Composites

sample	1st cycle discharge capacity [mAh/g]	1st cycle charge capacity [mAh/g]	columbic efficiency [%]	overall ICL [mAh/g]	ICL due to reduction of tin oxide to tin [mAh/g]	ICL due to SEI formation [mAh/g]
SO	1340.0	614.3	45.8	725.7	300.0	425.7
SO/LTO-5	1155.2	689.2	59.7	466.0	294.6	171.4
SO/LTO-15	1030.9	600.0	58.2	430.9	271.4	159.5
SO/LTO-30	983.8	580.3	59.0	403.5	261.2	142.3

dx.doi.org/10.1021/cm301432w | Chem. Mater. 2012, 24, 3329−3334

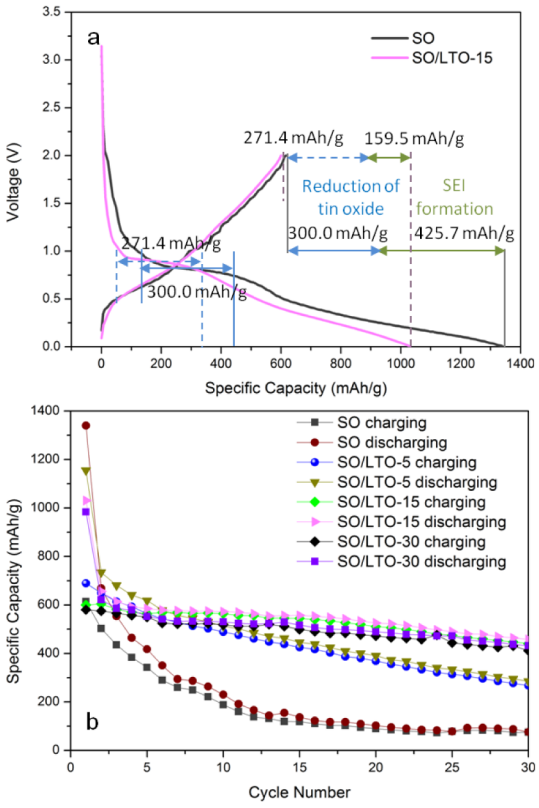

Figure 4. (a) Voltage profiles of SO and SO/LTO-15 at 100 mA/g and (b) cycling performance of SO, SO/LTO-5, SO/LTO-15, and SO/LTO-30 at 100 mA/g.

for SO/LTO-15. Hence a LTO coating could reduce the ICL associated with SEI formation by as much as 62.5%. This is confirmation that a lithium titanate coating could effectively reduce losses associated with SEI formation on Sn surfaces. However, the value of ICL is still higher than the ICL on LTO in the literature,[34] suggesting that some tin oxide was still exposed to the electrolyte. Because of the low specific capacity of LTO, composite particles with thicker shell thickness would result in lower discharge capacities, which is evident in Table 1. The ICL due to SEI formation for SO/LTO-5 and SO/LTO-30 were 171.4 and 142.3 mAh/g, respectively. The effect of shell thickness on ICL due to SEI formation was therefore not very significant. This suggests that a dense LTO layer which could satisfactorily insulate the underlying tin surface from the contact with electrolyte. It also implies the LTO coating should be as thin as possible from the aforementioned specific capacity considerations. The thinnest LTO that could be formed and delivered the ICL reduction functionality in this study was ~5 nm in thickness (i.e., SO/LTO-5).

The cycling performance of the composites was also measured at 100 mA/g and Figure 4b shows their comparison. (The discharge and charge curves for all of the products in the first, second, fifth and 30th cycle are given in Supporting Information as Figure S4). The presence of a LTO coating was also found to improve the cycling performance of hollow tin oxide NPs. For example, the discharge capacity of uncoated hollow tin oxide NPs decreased to 75.6 mAh/g by the 30th cycle whereas the corresponding value for SO/LTO-5 was 284.8 mAh/g. This could probably be attributed to the quality of the SEI formed on LTO. However, the LTO shell in the current implementation was not totally resistant to the volume excursion in the core area; and hence exfoliation of the LTO coating could occur during cycling. This was most noticeable for SO/LTO-5 which had the thinnest LTO coating. For SO/LTO-15 and SO/LTO-30, the discharge capacities were 656.7 and 621.5 mAh/g in the second cycle, and decreased to 457.1 and 431.5 mAh/g in the 30th cycle. The better performance of SO/LTO-15 and SO/LTO-30 relative to SO/LTO-5 was clearly a shell thickness effect. The specific capacity of SO/LTO-15 was higher than that of SO/LTO-30 because of its lower LTO content. Although capacity decay could still be observed, the cycling performance of tin oxide NPs with LTO coating layer showed significant improvements over the uncoated tin oxide NPs. The capacity decay was mostly caused by the exfoliation of the LTO coating layer after repetitive expansion and contraction of the anode. We believe through further work, the LTO coating can be optimized to provide a more stable cycling performance.

The cyclic voltammograms (CVs) of hollow tin oxide NPs and SO/LTO-15 in Supporting Information Figure S2 show the electrochemical changes that occurred in the initial cycling of these materials. In the first cycle, two cathodic peaks corresponding to reduction of tin oxide to tin and the lithiation of tin appeared at 0.5 and 0.01 V for pristine SnO_2; and at 0.64 and 0.07 V for the SO/LTO-15 composite.[41] The shift could be attributed to the facilitated transport of Li^+ through the LTO layer. A feeble cathodic peak at 1.5 V for SO/LTO-15 in the first cycle could be due to Li^+ intercalation into LTO.[34] The peak corresponding to the reduction of tin oxide to tin was greatly reduced in the second and third cycles. The broad cathodic feature in the 1.3 − 0.8 V region may be assigned to SEI formation. It was more subdued in SO/LTO-15, indicating a lower extent of SEI formation on the LTO coated composite. The prominent anodic peak at ~0.6 V common to both electrodes may be attributed to the delithiation reaction. The other anodic peak at 1.0−1.8 V is likely to be due to the decomposition of Li_2O.[1,40,41]

The cycling performance of SO/LTO-15 at the higher current densities of 200 and 1000 mA/g is shown in Figure 5. The uncoated tin oxide NPs was unable to release the stored Li^+ at these high current densities. Similar discharge/charge capacities were obtained. Despite some increase in the ICL at 1000 mA/g, an average discharge capacity of 439 mA/g was available for at least 30 cycles at this high current density. Such

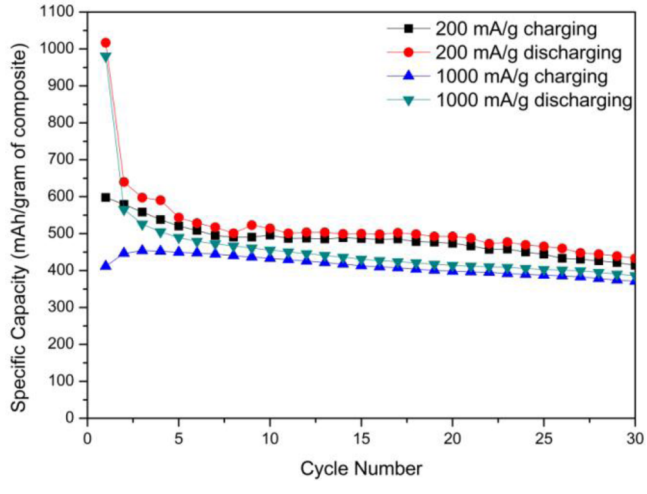

Figure 5. Cycling performance of SO/LTO-15 at 200 and 1000 mA/g.

dx.doi.org/10.1021/cm301432w | *Chem. Mater.* 2012, 24, 3329−3334

display of good rate performance could be due to the LTO coating acting as a funnel to draw the Li^+ toward the active material.[42] The structural stability of the composite was examined by comparing the morphology of the SO/LTO-15 electrode before and after 30 cycles. (Supporting Information, Figure S3) The results showed good retention of the overall spherical morphology without indication of shell rupture. This may be attributed to the containment effect of the LTO layer: keeping the tin based material within the hollow core area while the free volume in the latter accommodated the volume changes in cycling.

4. CONCLUSIONS

In conclusion, SnO_2@$Li_4Ti_5O_{12}$ core−shell composite particles with different shell thicknesses were prepared, which improved the electrochemical performance of the uncoated particles. The coating was effective in reducing the ICL because of SEI formation on the anode surface. Specifically a LTO coating on hollow tin oxide nanoparticle aggregates could lower the ICL for SEI formation from 425.7 mAh/g to 142.3 mAh/g. The cycling performance of hollow SnO_2@$Li_4Ti_5O_{12}$ was also a significant improvement over the pristine uncoated hollow tin oxide NPs. The discharge capacity of hollow tin oxide particles was only 75.6 mAh/g in the 30th cycle whereas the corresponding value for SO/LTO-15 was 457.1 mAh/g. Unlike some other studies, the specific capacities were calculated based on the weights of the composites, and not the weights of active materials only. A LTO layer ∼5 nm in thickness was sufficient to shield the contact between tin oxide and electrolyte. However, thicker LTO layers were more resistant to exfoliation caused by the volume excursion of the core material during cycling. Hence there exists some optimal shell thickness which balances the two opposing effects. Moreover, the LTO layers were also found to improve the rate capability of the active material. The LTO coating method is generic; and can be a new strategy for improving the electrochemical performance of other high capacity anode materials.

■ ASSOCIATED CONTENT

Ⓢ Supporting Information

EDX line scan images, cyclic voltammograms, SEM micrographs of sample before and after cycling, discharge and charge curves. This material is available free of charge via the Internet at http://pubs.acs.org.

■ AUTHOR INFORMATION

Corresponding Author

*E-mail: cheleejy@nus.edu.sg.

Notes

The authors declare no competing financial interest.

■ ACKNOWLEDGMENTS

G.J. gratefully acknowledges the National University of Singapore for her research scholarship. The Super P used in this project was provided free by Timcal.

■ REFERENCES

(1) Han, S. J.; Jang, B. C.; Kim, T.; Oh, S. M.; Hyeon, T. *Adv. Funct. Mater.* **2005**, *15*, 1845.
(2) Kim, C.; Noh, M.; Choi, M.; Cho, J.; Park, B. *Chem. Mater.* **2005**, *17*, 3297.
(3) Lou, X. W.; Wang, Y.; Yuan, C. L.; Lee, J. Y.; Archer, L. A. *Adv. Mater.* **2006**, *18*, 2325.
(4) Sun, X. M.; Liu, J. F.; Li, Y. D. *Chem. Mater.* **2006**, *18*, 3486.
(5) Bridel, J. S.; Grugeon, S.; Laruelle, S.; Hassoun, J.; Reale, P.; Scrosati, B.; Tarascon, J. M. *J. Power Sources* **2010**, *195*, 2036.
(6) Yang, J.; Winter, M.; Besenhard, J. O. *Solid State Ionics* **1996**, *90*, 281.
(7) Wang, Y.; Lee, J. Y. *Angew. Chem., Int. Ed.* **2006**, *45*, 7039.
(8) Wang, Y.; Zeng, H. C.; Lee, J. Y. *Adv. Mater.* **2006**, *18*, 645.
(9) Derrien, G.; Hassoun, J.; Panero, S.; Scrosati, B. *Adv. Mater.* **2007**, *19*, 2336.
(10) Park, M. S.; Wang, G. X.; Kang, Y. M.; Wexler, D.; Dou, S. X.; Liu, H. K. *Angew. Chem., Int. Ed.* **2007**, *46*, 750.
(11) Yu, Y.; Chen, C. H.; Shi, Y. *Adv. Mater.* **2007**, *19*, 993.
(12) Chan, C. K.; Peng, H. L.; Liu, G.; McIlwrath, K.; Zhang, X. F.; Huggins, R. A.; Cui, Y. *Nat. Nanotechnol.* **2008**, *3*, 31.
(13) Chen, G.; Wang, Z.; Xia, D. *Chem. Mater.* **2008**, *20*, 6951.
(14) Deng, D.; Lee, J. Y. *Chem. Mater.* **2008**, *20*, 1841.
(15) Kim, H.; Cho, J. *J. Mater. Chem.* **2008**, *18*, 771.
(16) Kim, H.; Han, B.; Choo, J.; Cho, J. *Angew. Chem., Int. Ed.* **2008**, *47*, 10151.
(17) Deng, D.; Lee, J. Y. *Angew. Chem., Int. Ed.* **2009**, *48*, 1660.
(18) Cui, G. L.; Hu, Y. S.; Zhi, L. J.; Wu, D. Q.; Lieberwirth, I.; Maier, J.; Mullen, K. *Small* **2007**, *3*, 2066.
(19) Lee, H.; Kim, H.; Doo, S. G.; Cho, J. *J. Electrochem. Soc.* **2007**, *154*, A343.
(20) Kim, H.; Cho, J. *Chem. Mater.* **2008**, *20*, 1679.
(21) Noh, M.; Kwon, Y.; Lee, H.; Cho, J.; Kim, Y.; Kim, M. G. *Chem. Mater.* **2005**, *17*, 1926.
(22) Wang, Y.; Su, F.; Lee, J. Y.; Zhao, X. S. *Chem. Mater.* **2006**, *18*, 1347.
(23) Cho, J. *Electrochim. Acta* **2008**, *54*, 461.
(24) Kim, H.; Cho, J. *Nano Lett.* **2008**, *8*, 3688.
(25) Kwon, Y.; Cho, J. *Chem. Commun.* **2008**, 1109.
(26) Lou, X. W.; Chen, J. S.; Chen, P.; Archer, L. A. *Chem. Mater.* **2009**, *21*, 2868.
(27) Lou, X. W.; Li, C. M.; Archer, L. A. *Adv. Mater.* **2009**, *21*, 2536.
(28) Deng, D.; Lee, J. Y. *J. Mater. Chem.* **2010**, *20*, 8045.
(29) Chen, J. S.; Luan, D.; Li, C. M.; Boey, F. Y. C.; Qiao, S.; Lou, X. W. *Chem. Commun.* **2010**, *46*, 8252.
(30) Lee, W. J.; Park, M. H.; Wang, Y.; Lee, J. Y.; Cho, J. *Chem. Commun.* **2010**, *46*, 622.
(31) Courtney, I. A.; Dahn, J. R. *J. Electrochem. Soc.* **1997**, *144*, 2045.
(32) Jiang, C. H.; Zhou, Y.; Honma, I.; Kudo, T.; Zhou, H. S. *J. Power Sources* **2007**, *166*, 514.
(33) Shu, J. *Electrochem. Solid State Lett.* **2008**, *11*, A238.
(34) Shu, J. *J. Solid State Electrochem.* **2009**, *13*, 1535.
(35) Wang, Y. Y.; Hao, Y. J.; Lai, Q. Y.; Lu, J. Z.; Chen, Y. D.; Ji, X. Y. *Ionics* **2008**, *14*, 85.
(36) Cai, R.; Yu, X.; Liu, X.; Shao, Z. *J. Power Sources* **2010**, *195*, 8244.
(37) Sivashanmugam, A.; Gopukumar, S.; Thirunakaran, R.; Nithya, C.; Prema, S. *Mater. Res. Bull.* **2011**, *46*, 492.
(38) Wagemaker, M.; van Eck, E. R. H.; Kentgens, A. P. M.; Mulder, F. M. *J. Phys. Chem. B* **2008**, *113*, 224.
(39) Wang, P.; Chen, D.; Tang, F. Q. *Langmuir* **2006**, *22*, 4832.
(40) Demir-Cakan, R.; Hu, Y. S.; Antonietti, M.; Maier, J.; Titirici, M. M. *Chem. Mater.* **2008**, *20*, 1227.
(41) Aurbach, D.; Nimberger, A.; Markovsky, B.; Levi, E.; Sominski, E.; Gedanken, A. *Chem. Mater.* **2002**, *14*, 4155.
(42) Reitmeier, S. J.; Gobin, O. C.; Jentys, A.; Lercher, J. A. *Angew. Chem., Int. Ed.* **2009**, *48*, 533.